Microsystem Technologies (2018) 24:4631–4639
https://doi.org/10.1007/s00542-018-3858-6

TECHNICAL PAPER

Biaxial scanning mirror with large rotation angle and low resonance frequency for LIDAR application

Buhyun Shin[1] · Dongho Oh[2] · Kyung-min Lee[2]

Received: 30 October 2017 / Accepted: 18 March 2018 / Published online: 27 March 2018

Abstract
We propose a biaxial scanning mirror with a large rotation angle and low resonance frequency for a compact and low-power-consuming LIDAR. The scanning mirror in LIDAR, which is driven by a rotating motor, requires a wide field of view and a low working frequency. To achieve these requirements, we develop an electromagnetic actuator for a biaxial scanning mirror that consists of two pairs of coils, one yoke with a cross shape, one rare-earth permanent magnet, and one gimbal structure frame. The gap distance between the permanent magnet and yoke is adjusted to find the optimum condition. The overall size of the developed system is 20 mm × 20 mm × 12 mm (width × depth × height) with a gap distance of 3 mm. Experiments and simulations are performed with various gap distances. The experimental results indicate that the maximum rotation angle is ± 51° at 37 Hz when the gap distance is 3 mm and the applied voltage is ± 5 V.

1 Introduction

A LIDAR is an apparatus that measures the distance to a target by using pulsed laser light. It is widely used in mobile applications to detect obstacles, avoid collisions, and navigate safely. Mobile applications demand compact and low-power-consuming devices to minimize the weight, volume, and battery consumption. One of the key components in LIDAR is a scanning mirror, which is driven by a bulky and heavy rotating motor. Recently, some efforts have been made to replace the rotating motor with an MEMS scanning mirror to make the rotating system compact and light (Mizuno et al. 2008; Sandner et al. 2010; Kimoto et al. 2014).

A LIDAR requires a wide field of view (FOV), usually greater than 180°, and a working frequency varying between approximately 20–100 Hz (online catalogue of LIDAR, https://sick-virginia.data.continum.net/media/docs/6/66/166/Product_information_LMS5xx_Laser_Measurement_Technology_en_IM0038166.PDF). As the working frequency increases, the angular resolution decreases under a given sampling frequency, because the scanning mirror in LIDAR not only transmits light but also receives the reflected light to measure the distance to an object. The rotating mirror should be sufficiently large to reflect a laser beam spot. Thus, the existing LIDAR systems use a rotating motor for the rotation of a scanning mirror. A bulky motor and rotating structure are obstacles to a compact and lightweight LIDAR. In addition, there are other disadvantages of a rotating motor, including high power consumption, large rotational inertia moment, and high cost.

MEMS scanning mirrors have a small size and low power consumption and achieve significant deflection at a resonance frequency (Holmström et al. 2014). MEMS scanning mirror driven by pressure actuators has a rotation angle of 75°, and PZT-driven MEMS scanning mirrors have a rotation angle of 27° and ± 38.9° (Werber and Zappe 2006; Iseki et al. 2010; Koh et al. 2011). An electromagnetically driven MEMS scanner has a ϕ 2.5 mm mirror, but its rotation angle is too small (Iseki et al. 2006). The rotation angles are insufficient and the resonance frequencies are high for LIDAR applications. A scanning mirror with mechanically rotating joints of ± 40° and ± 20° at the x- and y-axes at 60 Hz, respectively, was developed (Shin et al. 2013). However, it has a large and unsymmetrical structure, which makes it difficult to control. There are many other studies on scanning mirrors, but the maximum deflection angles of most scanning mirrors

✉ Kyung-min Lee
lee.km@cnu.ac.kr

[1] Department of Mechanical Engineering, Hanbat National University, Daejeon, Korea

[2] School of Mechanical Engineering, Chungnam National University, Daejeon, Korea

have been limited to 40°. Further, the deflection angle results from the deformation of the structure at high frequencies, which is not preferred for LIDAR applications (Pengwang et al. 2016). Recently, studies have been conducted on increasing scanning angle by using lenses, Snell's windows, and wedge-shape optic amplifiers for LIDAR application (Milanović et al. 2011; Hofmann et al. 2012; Zhang et al. 2016; Ye et al. 2016). Other studies have used an electromagnetic actuator to increase the scanning angle (Ataman et al. 2012). However, the deflection angles are still insufficient.

In this study, we developed a biaxial scanning mirror with a large rotation angle and a low resonance frequency for a compact and low-power-consuming LIDAR. To achieve the requirements, we designed and developed a customized electromagnetic actuator as the driving mechanism and investigated the effect of the gap distance on the performances. In Sect. 2, the design and working principles of the developed biaxial scanning mirror and electromagnetic actuator are described. In Sect. 3, we provide the simulation results of the designed actuator while varying the gap distance between the permanent magnet and yoke. In Sect. 4, experiments carried out to verify the proposed theory and simulation results are described in detail.

2 Design of biaxial scanning mirror for LIDAR application

A LIDAR typically needs an FOV greater than 180° and a rotating frequency varying between 25 and 100 Hz. The optical reflection angle of the mirror is twice the rotation angle of the mirror and the mirror scans twice in one cycle. Therefore, the required rotation angle and resonance frequency were set to 95° (= ± 47.5°) and approximately 40 Hz, respectively. For a large rotation angle and low resonance frequency, an electromagnetic actuator with rotating joints was selected because an electromagnetic actuator shows a relatively large rotation angle compared with other actuators in previous study (Shin et al. 2013).

We designed a biaxial scanning mirror with a gimbal structure driven by an electromagnetic force. Figure 1 shows the developed biaxial scanning mirror and its working principle. It consists of a moving part at the top and a stationary part at the bottom. The stationary part consists of one bottom plate, four supports, and two pairs of coils around one yoke with a cross shape. The moving part consists of one gimbal structure supported by four supports and one permanent magnet. The detailed properties and dimensions are listed in Table 1. The permanent

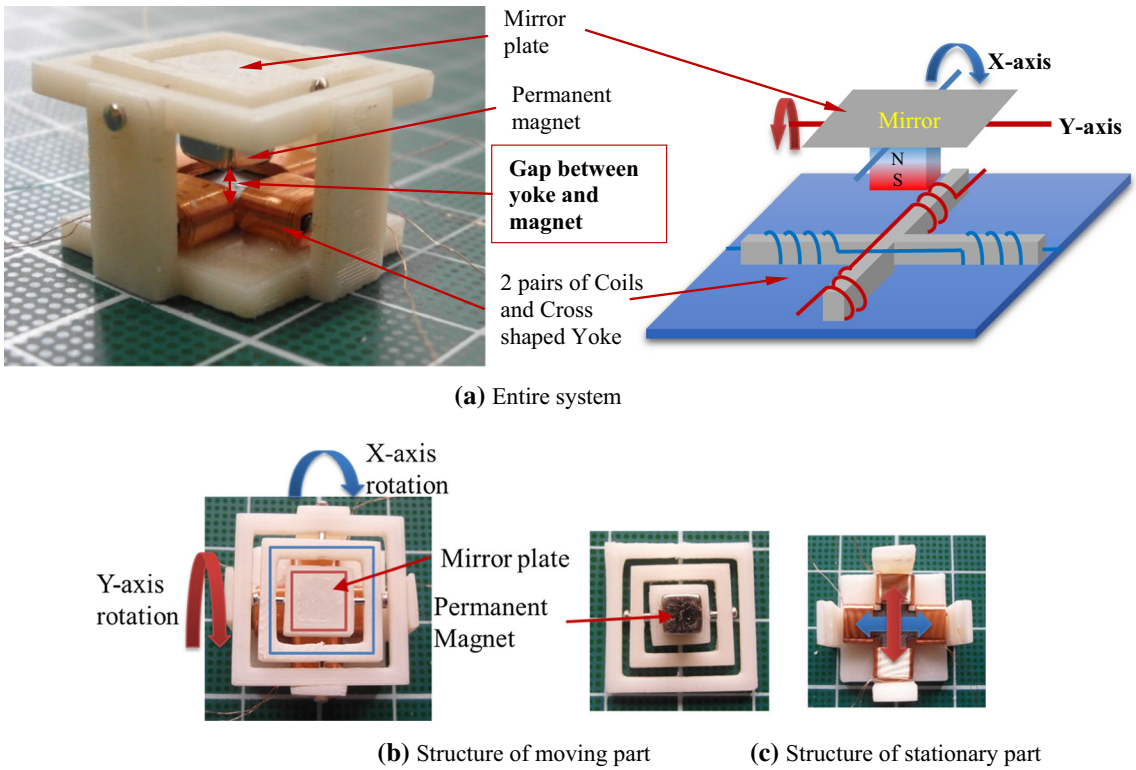

(a) Entire system

(b) Structure of moving part **(c)** Structure of stationary part

Fig. 1 Structure and working principle of the developed biaxial scanning mirror (color figure online)

Table 1 Parameter values

Parameter	Value
Size	
Entire system	20 × 20 × (11–15) mm
Gimbal structure	16 × 16 mm
Mirror plate on the gimbal structure	8 × 8 mm
Inertia (J)—X, Y axis	1.9×10^{-8}, 1.4×10^{-8} kg m^2
Resister (R)	116 Ω (a pair of two coils in series, 1620 turns)
Permanent magnet	Neodymium (ND50)
Yoke with cross shape	S45C

magnet is attached to the bottom of the center plate. The permanent magnet moves up and down according to the direction of the current, and as the current flows through the upper and lower coils (red coils in Fig. 1b), which are connected in series, the mirror rotates around the y-axis. When the current flows thorough the left and right coils (blue coils in Fig. 1b), the permanent magnet moves left and right according to the direction of the current. The mirror then rotates around the x-axis.

To achieve the requirements, we varied the gap distance between the permanent magnet and yoke. Theoretically, the mechanical and electrical performances, such as the torque constant, restoring torque constant, the geometric range of the rotation angle, and the resonance frequency are greatly affected by the gap distance among many parameters. When the gap distance decreases, which means the permanent magnet is closer to the yoke and coils, the restoring torque and rotating torque increase. The resonance frequency, which is a function of the rotating torque, restoring torque constant, and other values, also changes. Here, we investigate the relationship between the gap distance and mechanical and electrical properties while varying the gap distance from 2 to 6 mm at 1 mm intervals.

3 Simulation

For the theoretical analysis, the mechanical and electrical equations were derived from the equations of a DC motor, as shown in Eq. (1):

$$\begin{aligned} &J\ddot{\theta} + T_{magnet} = T_{electromagnet} \\ &T_{magnet} = K_m\theta,\ T_{electromagnet} = K_t I. \\ &V = RI + K_e\dot{\theta} \end{aligned} \tag{1}$$

Here, J is the mass moment of inertia; $\ddot{\theta}$, $\dot{\theta}$ and θ are the angular acceleration, angular velocity, and rotation angle; T_{magnet} is the restoring torque that rotates the permanent magnet to a neutral position; $T_{electromagnet}$ is the torque that rotates the permanent magnet to a certain angle; K_m and K_t are the restoring torque constant and the torque constant, respectively; I is the current flowing through the coils; V is the applied voltage; R is the resistance of the coil; and K_e is the back-EMF constant.

The relationship between the rotation angle and applied voltage is calculated from the Eq. (1) as:

$$\frac{\theta}{V} = \frac{1}{\frac{JR}{K_t}s^2 + K_e s + \frac{K_m R}{K_t}}. \tag{2}$$

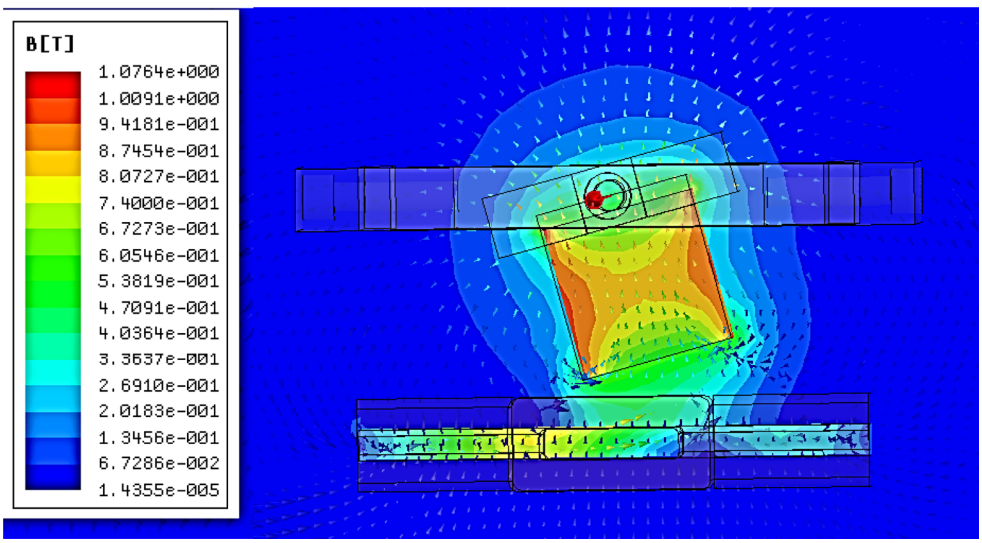

Fig. 2 Simulation results of the permanent magnet torque with 2 mm gap distance

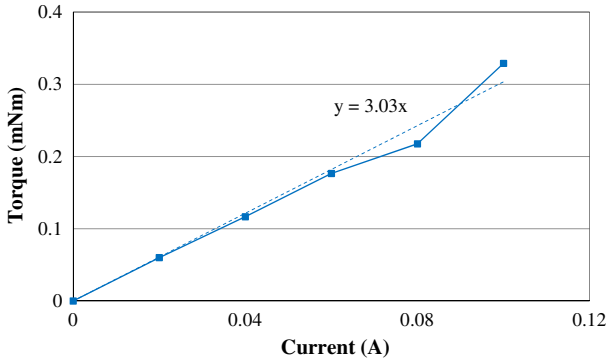

(a) Relation between torque and current at gap distance of 3 mm

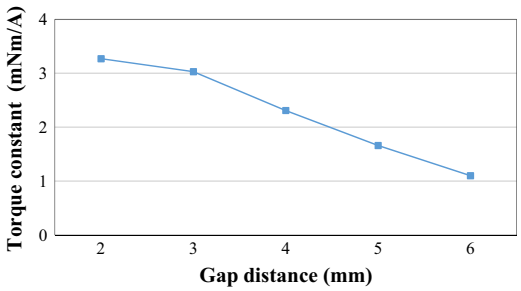

(b) Relation between torque constant and gap distance

Fig. 3 Simulated torque and torque constants

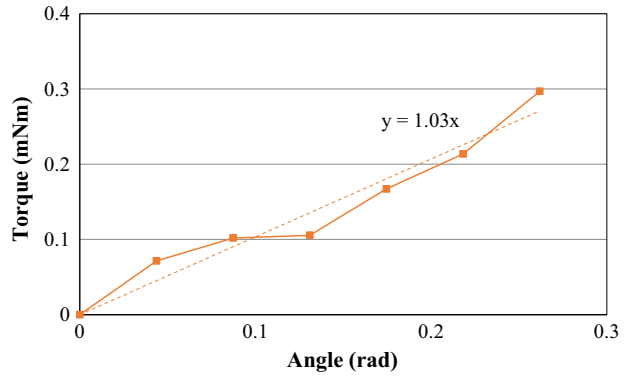

(a) Relation between restoring torque and rotation angle at gap distance of 3 mm

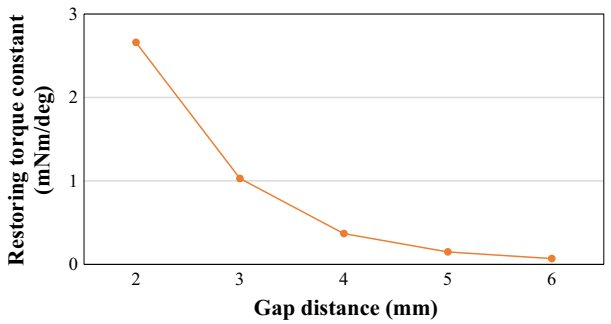

(b) Relation between restoring torque constant and gap distance

Fig. 4 Simulated restoring torque and restoring torque constants

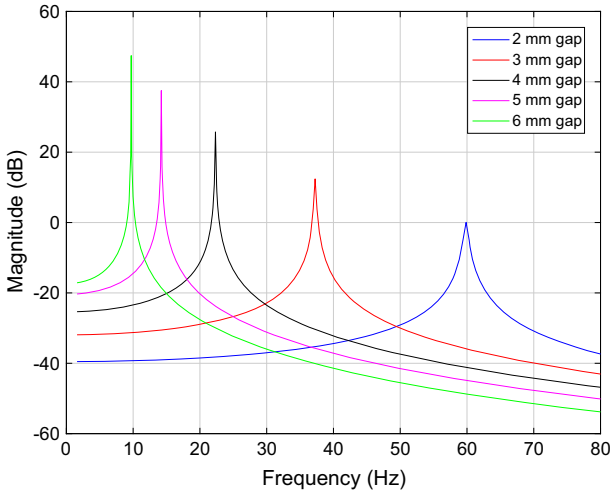

(a) Dynamic response of X-axis (outside)

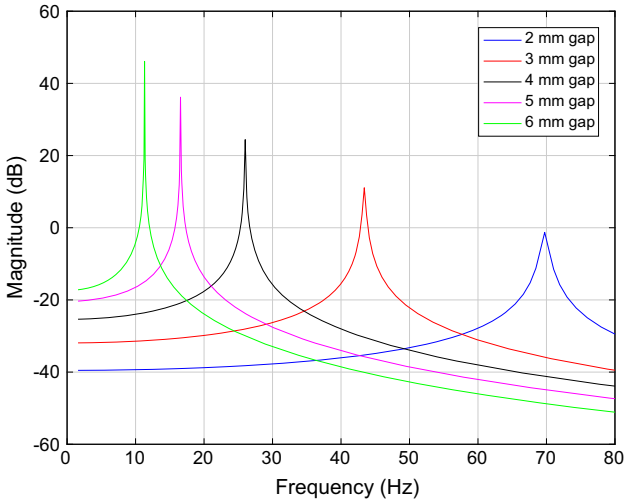

(b) Dynamic response of Y-axis (inside)

Fig. 5 Calculated dynamic responses

We conduct a finite element analysis (FEA) to calculate the restoring torque constants and the torque constants according to the gap distance by using a commercial software. Already-known material properties are used such as the B–H curve and magnets, and other parameters for simulation are measured from the prototype such as resistance and inertia. Figure 2 shows the simulation results of the magnetic flux density when the gap distance is 2 mm and the rotation angle is 10°.

Figure 3 shows the simulated torque in the actuator at the gap distance of 3 mm and the relations between the torque constant and the gap distances. The torque constants were calculated from the slope of the lines. The torques are proportional to the current as expected in Eq. (1). The torque constants decreased as the gap distance increased. Figure 4 shows the simulated restoring torque in the

Table 2 Simulated torque constants, restoring torque constants, and related parameters according to the gap distance

Gap distance (mm)	K_t and K_e (mNm/A)	K_m (mNm/rad)	Rotating angle at ± 5 V (°)	Resonance freq. of X, Y-axis (Hz)
2	3.27	2.66	± 3.04	60, 69
3	3.03	1.03	± 7.27	37, 43
4	2.31	0.37	± 15.42	22, 26
5	1.66	0.15	± 27.33	14, 17
6	1.1	0.07	± 38.81	10, 11

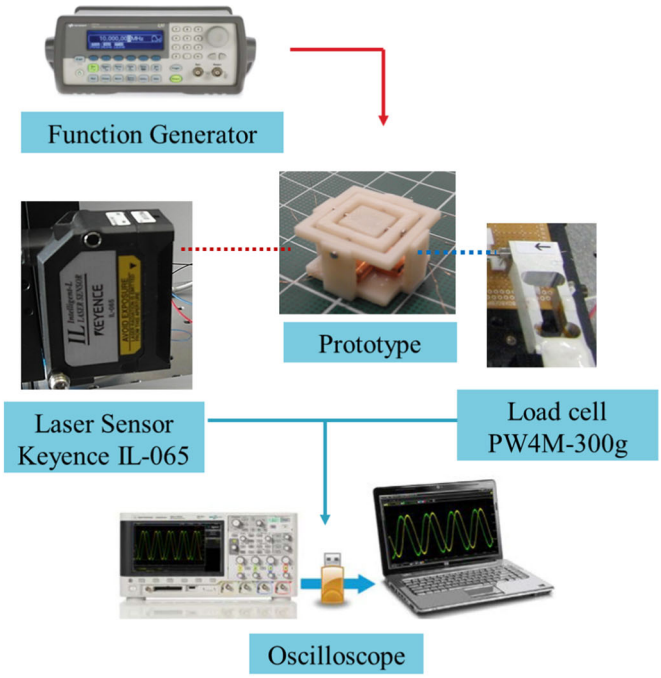

(a) Experimental setup

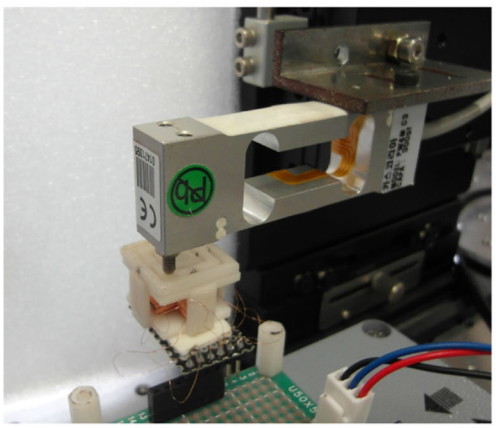

(b) Measure ment of torque

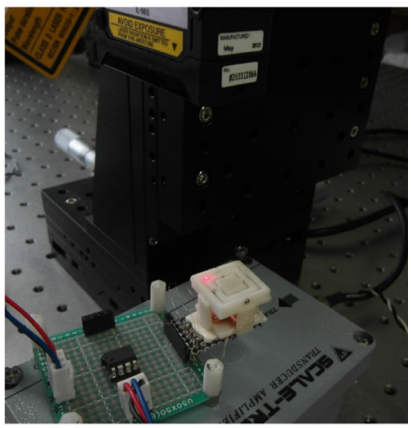

(c) Measurement of rotation angle

Fig. 6 Experimental setup of the developed biaxial scanning mirror

actuator according to the rotation angles from the neutral point and gap distances. The restoring torque constants were also calculated from the slope of the lines. The restoring torques are proportional to the angle, as shown in Eq. (1). However, the restoring torque constants decreased more rapidly than the torque constants as the gap distance

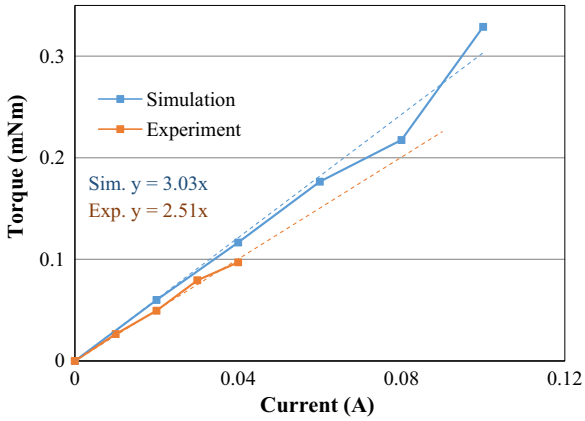

(a) Torque comparisons at 3-mm gap distance

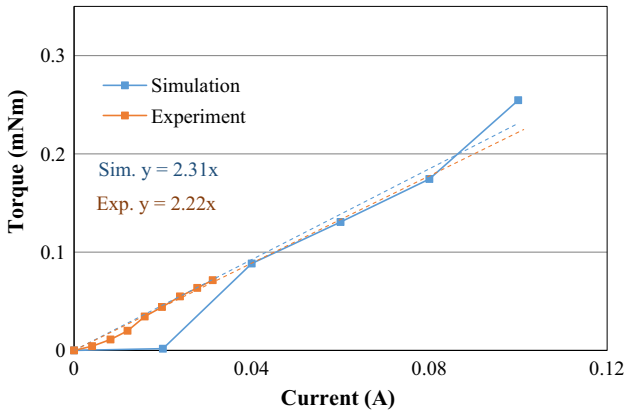

(b) Torques comparisons at 4-mm gap distance

Fig. 7 Comparison of torque

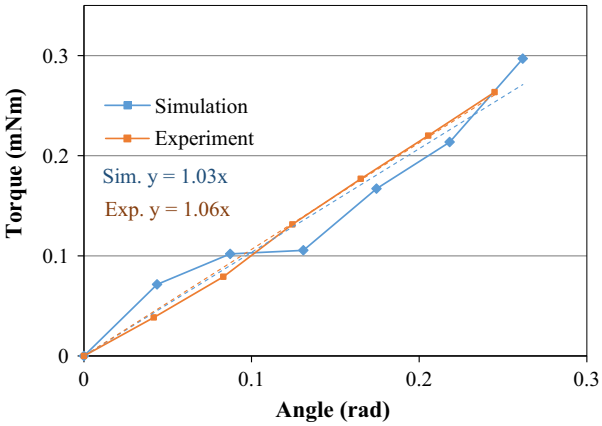

(a) Restoring torque comparison at 3-mm gap distance

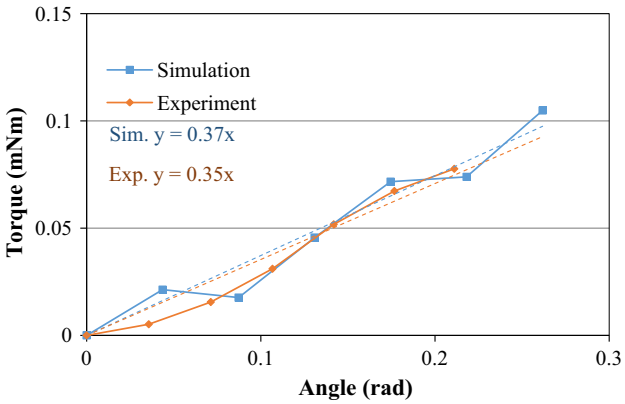

(b) Restoring torque comparison at 4-mm gap distance

Fig. 8 Comparison of restoring torque

increased, which means that the restoring torque is dominant at smaller gap distance relatively. From the results and Eq. (2), it is expected that the resonance frequency will decrease as the gap distance increase:

$$\theta = \frac{K_t}{K_m} I = \frac{K_t}{K_m} \cdot \frac{V}{R} (rad). \tag{3}$$

From the Eq. (3), the maximum rotation angle at the given voltage input was calculated. The calculated maximum rotation angle with a 3-mm gap distance at 5 V was 7.27°, which was much smaller than the required value.

Next, we calculated the resonance frequencies and magnitude. The magnitude provides information on the rotation angle amplification at the resonance frequency. The dynamic responses derived from Eq. (2) are shown in Fig. 5. The resonance frequencies of the x- and y-axes are slightly different owing to the difference in the mass moment of inertia of the two axis. The resonance frequencies decrease and the magnitudes increase as the gap distance increases as expected. The resonance frequencies were approximately 40 Hz with a 3-mm gap distance. Table 2 summarize the simulation results.

4 Experiment

The prototype manufactured is shown in Fig. 1. The gap distance was adjusted by changing the length of four supports. Figure 6 shows the experimental setup. The actuator was controlled using an open-loop control circuit with a power op-amp. The input signal was generated using a function generator. A load cell (CAStm PW4M C3) measured the force at the mirror plate or rotating structure, and the laser displacement sensor (Keyence IL-065) measured the vertical displacement of the mirror plate and rotating structure. The torque was calculated from the forces measured at the mirror plate and the rotating structure when input currents were applied. The restoring torque was calculated from the restoring forces measured at the mirror plate and the rotating structure when the structure was rotated from a neutral position.

The torque constants and restoring torque constants at each gap distance were calculated. When the gap distance was 2 mm, the mirror does not rotate at 5 V owing to the large restoring torque. Thus, the gap distances are varied from 3 to 6 mm at intervals of 1 mm. The torque constant

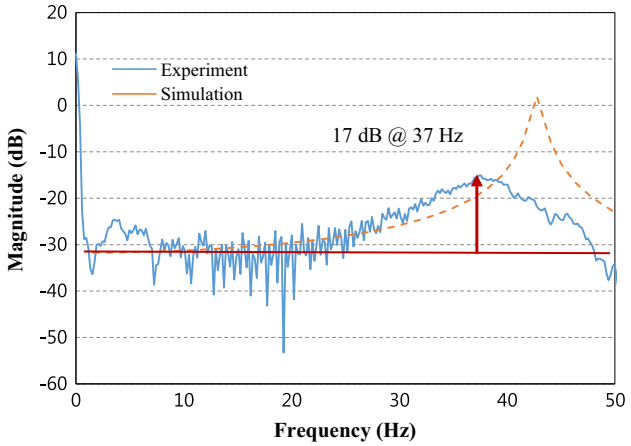

(a) Dynamic response at 3-mm gap distance

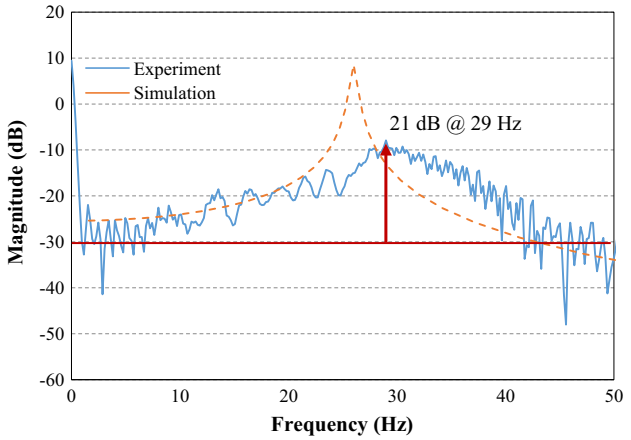

(b) Dynamic response at 4-mm gap distance

Fig. 9 Dynamic responses of y-axis (inside) according to the gap distance

was the slope of the current–torque relation shown in Fig. 7. The restoring torque constant was the slope of the angle–torque relation shown in Fig. 8. The experimental results were compared with the simulation results shown in Figs. 7 and 8. The rotation angle was ± 5.6° with a 3-mm gap distance at ± 5 V, which was smaller than expected in simulation.

The dynamic responses of the developed system were measured to investigate the rotation angle at the resonance frequency. For the dynamic response, sinusoidal sweep excitation experiments were conducted. The range of the sweep frequency was 0.1–100 Hz and the amplitude was 5 V. Figure 9 compares the experimental and simulation results. The resonance frequency and magnitude of the Y-axis at a 3-mm gap distance were 37 Hz and 17 dB, respectively. The maximum rotation angle calculated from the magnitude and the rotation angle at ± 5 V is ± 40°, theoretically. The measured maximum rotation angle at the resonance frequency were ± 51° with a 3-mm gap distance, which is slightly higher than theoretical calculation. Considering the noise in the dynamic responses, this difference was acceptable. As a result, the optical reflection angle with a 3-mm gap distance at 37 Hz was 204° based on the experimental result, which satisfies the requirements for a compact LIDAR.

Table 3 summarizes the experimental results. They correspond with the simulation results. However, the torque constant does not decrease as expected as the gap distance increase. Thus, the rotation angles are large, and the resonance frequency is slightly lower in the experiments of the gap distance of 4 and 5 mm.

Horizontal and vertical beam profiles were scanned to verify the developed scanning mirror as shown in Fig. 10a, b. The input voltage was ± 1.5 V, and the frequency was 10 Hz.

From the Eq. (1), we calculated the rotation angle when a sinusoidal signal was applied:

$$J\ddot{\theta} + K_m\theta = \frac{K_t}{R}V_0 sin(2\pi ft), \tag{4}$$

$$\theta = \frac{\mathrm{K_t}V_0}{\mathrm{R}(\mathrm{K_m} - J(2\pi f)^2)}\left(\sin(2\pi ft) - \frac{2\pi \mathrm{f}}{\sqrt{\frac{k_m}{J}}}\sin\left(\sqrt{\frac{k_m}{J}}t\right)\right). \tag{5}$$

Here V_0 and f is the amplitude and frequency of the sinusoidal signals, respectively.

When the gap distance was 3 mm and the other conditions and boundary conditions were set at: $V_0 = 1.5\,\mathrm{V}$, $f = 5\,\mathrm{Hz}$, $\dot{\theta} = 0$ and $\theta = 0$. The rotation angles were calculated as:

$$\theta_x = 0.031\sin(31.4\mathrm{t}) + 0.0041\sin(236\mathrm{t})(\mathrm{rad}),$$

$$\theta_y = 0.031\sin(31.4\mathrm{t}) + 0.0035\sin(275\mathrm{t})(\mathrm{rad}).$$

Table 3 Torque constants, restoring torque constants, and related parameters according to the gap distance from Experiments

Gap distance (mm)	K_t and K_e (mNm/A)	K_m (mNm/rad)	Rotating angle at 5 V (°)	Resonance freq. of X, Y-axis (Hz)
3	2.51	1.06	± 5.6	29, 37
4	2.22	0.35	± 16.0	22, 29
5	2.0	0.12	± 41.2.	12, 14
6	1.4	0.05	± 69.2	7, 10

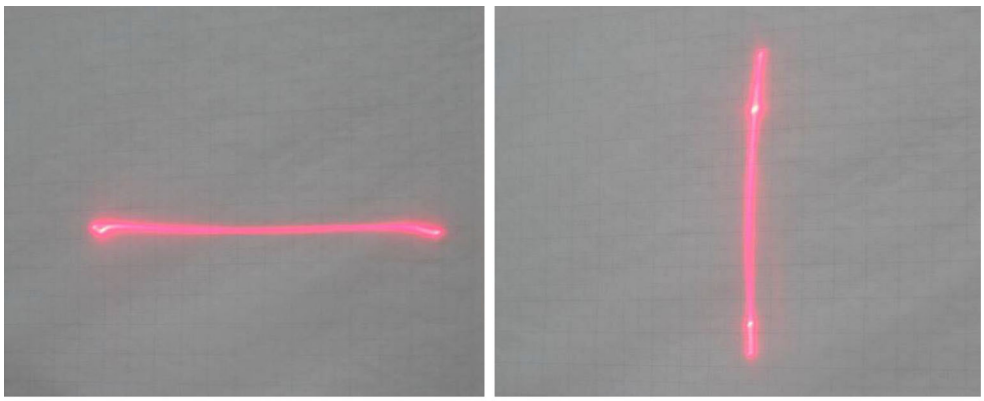

(a) Horizontal scanning **(b)** Vertical scanning

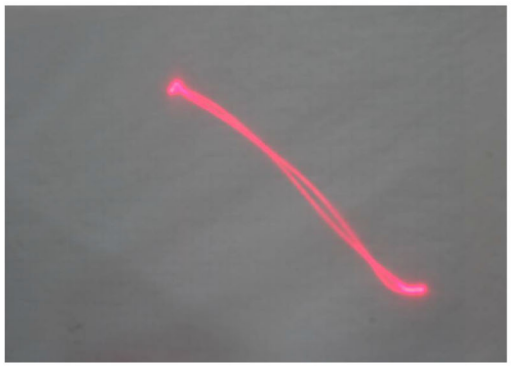

(c) Oblique scanning

Fig. 10 Scanning pattern of developed scanning mirror

The trajectories of the x and y axis were slightly different because of the homogenous solutions in the rotation angles. The scanning mirror drew an oscillating line along a 45° oblique line as shown in Fig. 10c. The amplitude of the homogenous solution increases as the frequency and the mass moment of inertia increase and the restoring torque constant decreases.

5 Conclusion

We developed a biaxial scanning mirror for a compact and low-power-consuming LIDAR system. To fulfil a large FOV at low resonance frequency, we designed and developed a customized electromagnetic actuator. It consists of one permanent magnet rotating with a gimbal structure and four electromagnets located in four directions on the base frame. We varied the gap distance from 2 to 6 mm at intervals of 1 mm and theoretically analyzed and simulated the performance of the developed electromagnetic actuator and the motion of the biaxial scanning mirror according to the gap distance. When the gap distance was 3 mm, the results satisfied the requirements for a LIDAR application with an optical reflection angle of 204° at a resonance frequency of 37 Hz. The results show that as the gap distance increases, the reflecting angle increases but the resonance frequency decrease. According to the requirement of LIDAR system, an appropriate gap distance can be calculated based on this experimental results in this study.

Table 4 compares the performance of the developed scanning mirror with other mirrors for LIDAR. The

Table 4 Comparison of scanning mirrors for LIDAR

Device	FOV (°)	Power input	Working frequency	Package size (mm)
Lee (lenses)	42.2 × 42.2	Double lenses		25 × 42 × 72
Zhang	150 (1-axis)	Snell's windows	2	1 $in.^3$
Ye	45 × 43	12.5 V	710 Hz @ 6.3 V	20 × 20 × 16
Ataman	10 × 10	12.8 V	170 Hz	4 × 4 × 3 (estimation)
Our work	102 × 102	5 V	29, 37 Hz (X, Y)	20 × 20 × 12

developed mirror satisfied the required specification with a wide FOV at a low resonance frequency. Additionally, it consumes less power, which is an indispensable characteristic in mobile applications owing to the permanent magnet and rotating joint.

Acknowledgements This work was partially supported by the National Research Foundation of Korea (NRF) Grant funded by the Korea government (Ministry of Science, ICT and Future Planning) (no. NRF-2017R1C1B5018324). This work was partially supported by Basic Science Research Program through the National Research Foundation funded by the Ministry of Education (NRF-2017R1D1A1B03033321).

References

Ataman Ç, Lani S, Noell W, de Rooij N (2012) A dual-axis pointing mirror with moving-magnet actuation. J Micromech Microeng. https://doi.org/10.1088/0960-1317/23/2/025002

Hofmann Y, Senger F, Soerensen F, Stenchly V, Jensen B, Janes J (2012) Biaxial resonant 7 mm-MEMS mirror for automotive LIDAR application. In: International conference on optical MEMS and nanophotonics, pp 150–151. https://doi.org/10.1109/omems.2012.6318847

Holmström ST, Baran U, Urey H (2014) MEMS laser scanners: a review. J Microelectromech Syst. https://doi.org/10.1109/jmems.2013.2295470

https://sick-virginia.data.continum.net/media/docs/6/66/166/Product_information_LMS5xx_Laser_Measurement_Technology_en_IM0038166.PDF. Accessed 23 Jan 2018

Iseki T, Okumura M, Sugawara T (2006) Two-dimensionally deflecting mirror using electromagnetic actuation. Opt Rev. https://doi.org/10.1007/s10043-006-0189-0

Iseki T, Okumura M, Sugawara T (2010) High-speed and wide-angle deflection optical MEMS scanner using piezoelectric actuation. IEEJ Trans Electr Electron Eng. https://doi.org/10.1002/tee.20542

Kimoto K, Asada N, Mori T, Hara Y, Ohya A (2014) Development of small size 3d LIDAR. In: Robotics and automation (ICRA), 2014 IEEE international conference on, pp 4620–4626. https://doi.org/10.1109/icra.2014.6907534

Koh KH, Kobayashi T, Lee C (2011) A 2-D MEMS scanning mirror based on dynamic mixed mode excitation of a piezoelectric PZT thin film S-shaped actuator. Opt Express. https://doi.org/10.1364/oe.19.013812

Milanović V, Kasturi A, Siu N, Radojiþiü M, Su Y (2011) "MEMSEye" for optical 3D tracking and imaging applications. In: 16th intentional solid-state sensors, actuators and microsystem conference, pp 1895–1898. https://doi.org/10.1109/transducers.2011.5969770

Mizuno T, Mita M, Kajikawa Y, Takeyama N, Ikeda H, Kawahara K (2008) Study of two-dimensional scanning LIDAR for planetary explorer. In: Proceedings of the SPIE, p 71061A-9. https://doi.org/10.1117/12.800791

Pengwang E, Rabenorosoa K, Rakotondrabe M, Andreff N (2016) Scanning micromirror platform based on MEMS technology for medical application. Micromachines. https://doi.org/10.3390/mi7020024

Sandner T, Grasshoff T, Wildenhain M, Schenk H (2010) Synchronized microscanner array for large aperture receiver optics of LIDAR systems. In: Proceedings of the SPIE, p 75940C-12. https://doi.org/10.1117/12.844923

Shin BH, Oh D, Lee SY (2013) A two-dimensional laser scanning mirror using motion-decoupling electromagnetic actuators. Sensors. https://doi.org/10.3390/s130404146

Werber A, Zappe H (2006) Tunable membrane-based, pneumatic micro-mirrors. J Opt A Pure Appl Opt. https://doi.org/10.1088/1464-4258/8/7/s03

Ye L, Zhang G, You Z, Zhang C (2016) A 2D resonant MEMS scanner with an ultra-compact wedge-like multiplied angle amplification for miniature LIDAR application. Sensors. https://doi.org/10.1109/icsens.2016.7808932

Zhang X, Koppal SJ, Zhang R, Zhou L, Butler E, Xie H (2016) Wide angle structured light with a scanning MEMS mirror in liquid. Opt Express. https://doi.org/10.1364/OE.24.003479